AGU PUBLICATIONS

JGR

Journal of Geophysical Research: Oceans

RESEARCH ARTICLE

10.1002/2014JC010320

Key Points:
- Increased ocean acidification with increased freshwater supply
- Glacial water containing carbonate ions partly lessens ocean acidification
- First comprehensive study of the winter carbonate system in Spitsbergen fjord

Correspondence to:
A. Fransson,
agneta.fransson@npolar.no

Citation:
Fransson, A., M. Chierici, D. Nomura, M. A. Granskog, S. Kristiansen, T. Martma, and G. Nehrke (2015), Effect of glacial drainage water on the CO_2 system and ocean acidification state in an Arctic tidewater-glacier fjord during two contrasting years, *J. Geophys. Res. Oceans*, *120*, 2413–2429, doi:10.1002/2014JC010320.

Received 16 JUL 2014
Accepted 28 JAN 2015
Accepted article online 3 FEB 2015
Published online 2 APR 2015

Effect of glacial drainage water on the CO_2 system and ocean acidification state in an Arctic tidewater-glacier fjord during two contrasting years

Agneta Fransson[1], Melissa Chierici[2,3], Daiki Nomura[1,4], Mats A. Granskog[1], Svein Kristiansen[5], Tõnu Martma[6], and Gernot Nehrke[7]

[1]Norwegian Polar Institute, Fram Centre, Tromsø, Norway, [2]Institute of Marine Research and the Fram Centre, Tromsø, Norway, [3]University Centre in Svalbard, Longyearbyen, Norway, [4]Institute of Low Temperature Science, Hokkaido University, Sapporo, Japan, [5]Department of Arctic and Marine Biology, University of Tromsø, Arctic University of Norway, Norway, [6]Institute of Geology, Tallinn University of Technology, Estonia, [7]Alfred Wegener Institute, Bremerhaven, Germany

Abstract In order to investigate the effect of glacial water on the CO_2 system in the fjord, we studied the variability of the total alkalinity (A_T), total dissolved inorganic carbon (C_T), dissolved inorganic nutrients, oxygen isotopic ratio ($\delta^{18}O$), and freshwater fractions from the glacier front to the outer Tempelfjorden on Spitsbergen in winter 2012 (January, March, and April) and 2013 (April) and summer/fall 2013 (September). The two contrasting years clearly showed that the influence of freshwater, mixing, and haline convection affected the chemical and physical characteristics of the fjord. The seasonal variability showed the lowest calcium carbonate saturation state (Ω) and pH values in March 2012 coinciding with the highest freshwater fractions. The highest Ω and pH were found in September 2013, mostly due to CO_2 uptake during primary production. Overall, we found that increased freshwater supply decreased Ω, pH, and A_T. On the other hand, we observed higher A_T relative to salinity in the freshwater end-member in the mild and rainy winter of 2012 (1142 μmol kg^{-1}) compared to A_T in 2013 (526 μmol kg^{-1}). Observations of calcite and dolomite crystals in the glacial ice suggested supply of carbonate-rich glacial drainage water to the fjord. This implies that winters with a large amount of glacial drainage water partly provide a lessening of further ocean acidification, which will also affect the air-sea CO_2 exchange.

1. Introduction

The Svalbard archipelago is the main fjord region in the Eurasian Arctic [*Cottier et al.*, 2010] of which about 60% is covered by glaciers. Most of the Svalbard fjords are affected by freshwater and sedimentation from glaciers and riverine inflow, as well as sea-ice dynamics from seasonal ice formation and melt [e.g., *Svendsen et al.*, 2002]. Moreover, many glaciers on Svalbard are retreating and have shown decreasing glacier volume [e.g., *Kohler et al.*, 2007; *Nuth et al.*, 2010; *Moholdt et al.*, 2010]. The volume decrease is mainly caused by top melting through warming and increased precipitation [e.g., *Kohler et al.*, 2007], thus increasing the freshwater supply to the nearby fjord and ocean. The West Spitsbergen region is also influenced by inflowing warm Atlantic water (AW). Increased intrusion of ocean heat to the fjord has the potential to melt the glacier fronts at tidewater glaciers, similar to the process explaining the increased melt off from marine-terminating fronts of the Greenland Ice Sheet [e.g., *Holland et al.*, 2008; *Hanna et al.*, 2009; *Rignot et al.*, 2010].

Ocean acidification (OA) is caused by the increase in ocean CO_2 due to uptake of atmospheric CO_2. This increase has caused a shift in the CO_2 (or carbonate) chemistry to a less basic state, resulting in a decrease in ocean pH and carbonate ion concentration [CO_3^{2-}] [e.g., *Raven et al.*, 2005; *Gattuso and Hansson*, 2011, and references therein]. Calcium carbonate ($CaCO_3$) saturation state (Ω) is commonly used to indicate a change in the CO_2 chemistry (and OA state) and the dissolution potential for solid $CaCO_3$, such as calcareous shells and skeleton of marine organisms. When $\Omega < 1$, solid $CaCO_3$ is chemically unstable and prone to dissolution (i.e., the waters are undersaturated with respect to the $CaCO_3$ mineral). In the Arctic, increased freshwater supply from sea-ice melt and river runoff have shown to decrease Ω and provide a positive feedback on OA [*Chierici and Fransson*, 2009; *Yamamoto-Kawai et al.*, 2009; *Fransson et al.*, 2013; *Robbins et al.*, 2013].

In addition, *Chierici and Fransson* [2009] found that the total alkalinity and $[CO_3^{2-}]$ decreased on the Arctic shelves due to elevated freshwater fractions from sea-ice melt and river runoff. Furthermore, large amounts of river water contribute also with organic matter, increasing CO_2 and decreasing pH, due to mineralization of organic carbon. Depending on the bedrock of the river drainage area, river runoff could affect the CO_2 system, and even the alkalinity, as a result of water drainage over calcareous or noncalcareous bedrock [e.g., *Hjalmarsson et al*., 2008; *Evans et al*., 2014; *Azetsu-Scott et al*., 2014]. In general, Arctic fjords are little investigated regarding the CO_2 chemistry and OA state in the water column, and there are only few studies of the CO_2 system in the Arctic, mainly in the NE Greenland fjords [e.g., *Sejr et al*., 2011]. Moreover, CO_2-system data on the full seasonal cycle, in particular, winter data are scarce in the Arctic, are required to investigate the drivers/controls on the CO_2 system and OA state. This information is also necessary to understand the future atmospheric CO_2-uptake potential in the Arctic.

Freshening of the Arctic is now occurring [e.g., *Morison et al*., 2012] and increasing melt of Arctic ice sheets and glaciers may have a profound local impact on the OA state. Several studies focus on the effect of sea-ice melt and river runoff on OA state in the Arctic and limited studies on the effect of glacial melt and drainage water. Here we report on the seasonal and interannual variability of the CO_2 system, nutrients, and freshwater fractions during 2 contrasting years in a Spitsbergen fjord. Moreover, we estimate the effect of glacial drainage water on the CO_2 system, OA state, and ocean CO_2 uptake in an Arctic tidewater-glacier fjord.

2. Study Area

Tempelfjorden is situated in the easternmost part of Isfjorden on the West-Spitsbergen shelf (Figure 1). Tempelfjorden is 14 km long and 5 km wide and covers an area of 57 km^2 [*Forwick et al*., 2010]. Moreover, Tempelfjorden is situated on the west coast of Spitsbergen (west facing), meaning that it is influenced by the inflow of transformed Atlantic

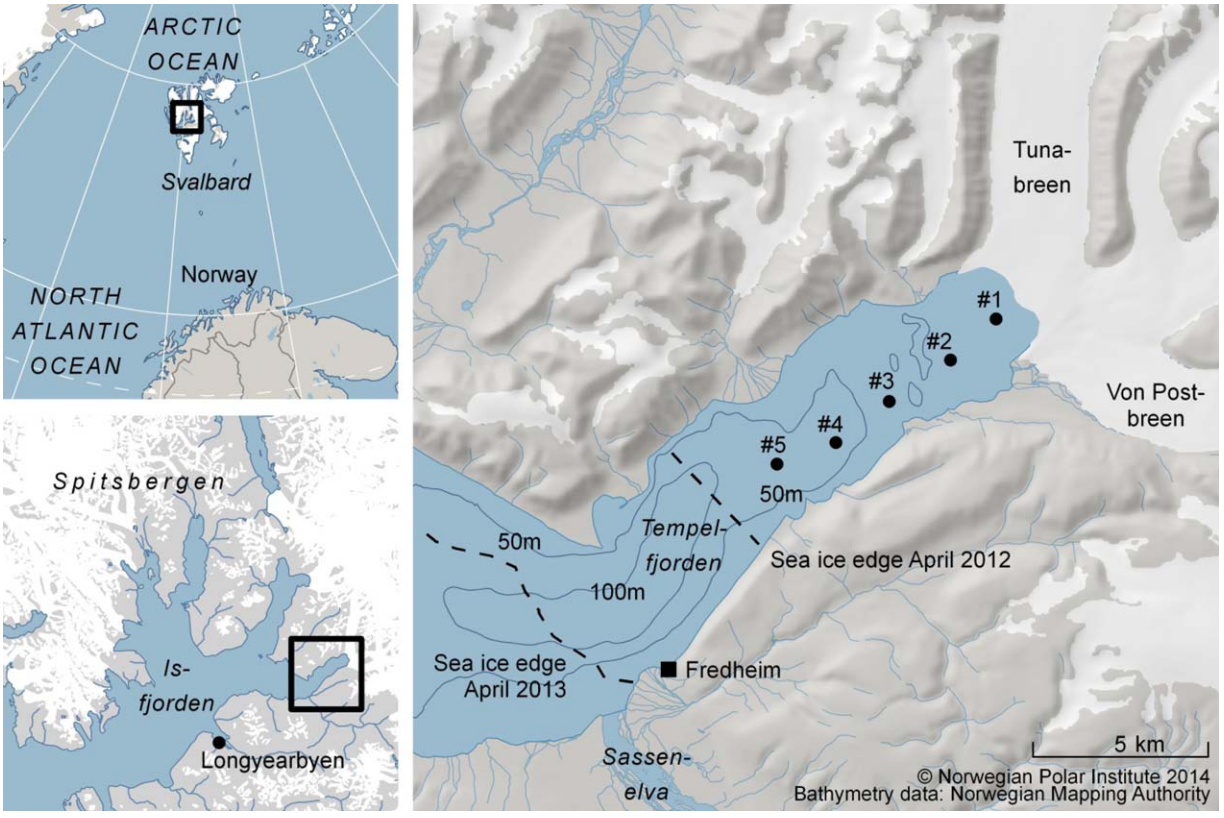

Figure 1. Map of study area and location (black dots) and number (#) of sampling stations in Tempelfjorden, northeast of Longyearbyen, Spitsbergen. Details on station locations and sampling dates are given in Table 1. The bathymetry of the fjord is marked by gray thin lines and depth in meters (m). Also marked on the map are the glaciers Tunabreen and Von Postbreen. The river mouth of Sassenelva is visible near Fredheim. The sea ice edge of the 2 years in winter is marked with dashed line. The dashed line near Fredheim is the sea ice edge in April 2012 (8.5 km from glacier front) and the one further out in the fjord mouth is in April 2013 (16 km from glacier front).

water, which is a relatively warm and saline water transported by the West Spitsbergen Current [e.g., *Nilsen et al.*, 2008]. Tempelfjorden is much less studied relative to many other fjords in Svalbard, for example, Kongsfjorden [e.g., *Svendsen et al.*, 2002; *Cottier et al.*, 2005; *Gerland and Renner*, 2007], Storfjorden [e.g., *Skogseth et al.*, 2005], and the adjacent Isfjorden [*Nilsen et al.*, 2008] which have been extensively studied mainly regarding their physical but also biological characteristics. Typically water masses in fjords consist of three layers; a fresh surface layer, an intermediate layer which is usually shelf water mixed with advected waters from the Atlantic, and cold deep water below the sill. Tempelfjorden is without a distinct sill (Figure 1) and the three-layer water mass arrangement is less distinct and show large seasonal and interannual variability, which was evident from our study.

Sea-ice formation in winter has the capacity to release high-salinity brine which induces water-column mixing or so called haline convection, creating a well-mixed high salinity and cold winter water [*Cottier et al.*, 2005]. Winter water is a mixture of transformed Atlantic water and freshwater exposed to large heat loss and wind mixing from fall to winter [*Nilsen et al.*, 2008]. In Tempelfjorden, sea ice usually starts to form in November and breaks up between April and July [*Svendsen et al.*, 2002; *Nilsen et al.*, 2008]. However, the timing of sea-ice formation and melt, as well as the location of the sea ice edge, has large interannual variability in western Spitsbergen fjords [*Cottier et al.*, 2007; *Gerland and Renner*, 2007]. In spring and summer sea-ice meltwater is introduced to the water column, although this may be a rather transient influence during the ice-melt period [*Cottier et al.*, 2010]. Fjords are different than the central Arctic Ocean, where the meltwater builds-up and has long retention time in the system. In fjords, the freshwater is flushed out quickly due to the fjord circulation [*MacLachlan et al.*, 2007].

The fjord is composed of two basins with a maximum water depth at 110 m in the main basin (central and outer fjord) and the smaller basin in the inner part of the fjord of a water depth up to 70 m (Figure 1). Our study took place in the inner part of the fjord (Figure 1). Two drainage basins surround the area and the northern drainage basin covers 785 km^2 and has a glacial coverage of 58% [*Hagen et al.*, 1993]. It composes of the calving tidewater glacier Tunabreen and the two land-terminating glaciers (von Postbreen and Bogebreen) at the head of Tempelfjorden (Figure 1). Tunabreen and von Postbreen are the major sediment sources in our study area (northern basin), and in the outer basin most particles in the freshwater originate from the Sassen River (Sassenelva).

The air temperature and precipitation data (at station Longyearbyen Airport) provided by the Norwegian Meteorological Institute (www.met.no) show that the period from December 2011 to March 2012 was significantly warmer than the long-term mean air temperature in 1964–2014. The air temperature anomaly from the long-term mean was $+12^{\circ}C$ in January 2012 and at the end of this month the precipitation was falling as rain, and it was an unusually mild winter with late sea-ice formation. In addition, the precipitation (as rain) in fall and winter (August–December) 2011 (preconditions for March/April 2012) was higher than the precipitation in fall/winter 2012 (preconditions for April 2013).

3. Data and Methods

3.1. Sampling

Table 1 summarizes the sampling dates and locations. In winter, we sampled fjord water from the upper water column (ice-water interface, 2, 5, 10, 15, and 20 m depths) at three to five stations from the glacier front to the outer parts of the fjord mouth (sea ice edge in 2012; Figure 1). The most extensive sampling was performed during April 2012 (five stations) and in April 2013 (four stations) and limited sampling were performed in January (one station near Fredheim, Figure 1), March 2012 (three stations) and in September 2013 (three stations; 1, 2, 10, 20, 30, and 40 m depths). In addition to the water column, we sampled glacial ice from the glacier front (winter time and September 2013) and at the beach (in September).

The fjord water from the upper water column was sampled using a polyethylene water sampling device of 0.5 L (in 2012) and 2.5 L (2013), immersed through the ice bore hole in winter, and in September 2013 immersed directly into the water (no sea ice). In 2012, water samples were collected directly into borosilicate glass bottles (250 mL) for the CO_2 system (i.e., carbonate system), nutrients in acid washed Nalgene® bottles (125 mL) and oxygen isotopic ratio ($\delta^{18}O$) in 25 mL Wheaton® HDPE bottles (sealed with Parafilm®). Due to cold and harsh conditions in 2013, as well as challenging transportation to the sampling sites, water samples were contained in unbreakable HDPE Nalgene® bottles (500 mL) and ice, snow, and glacial ice in plastic Zip-locks® bags. The water was immediately put into an insulated cooling box to prevent freezing of

Table 1. Summary of the Sampling Dates, Locations (See Also Figure 1) and Number of Water Samples That Were Sampled for Each Station (N)

Sampling Date dd mm yyyy	Stn#	Location	Station Latitude (°N)	Station Longitude (°E)	N
25 Jan 2012	Near Fredheim	Ice edge	78.04	16.92	2
21 Mar 2012	1	Glacier	78.44	17.38	3
	2		78.42	17.31	4
	3	Ice edge	78.42	17.23	3
11 Apr 2012	1	Glacier	78.44	17.36	4
	2		78.43	17.30	4
	3		78.42	17.22	4
	4		78.41	17.15	4
	5	Ice edge	78.41	17.07	4
12 Apr 2013	1	Glacier	78.44	17.36	5
	2		78.43	17.30	5
	4		78.41	17.15	5
	5	Near ice edge	78.41	17.07	5
18 Sep 2013	1	Glacier	78.44	17.36	6
	1b	Glacier	78.44	17.38	6
	5	Mid-fjord	78.41	17.07	6

the samples. Immediately after return to the laboratory at UNIS (Longyearbyen), the water samples for the determination of the CO_2 system were transferred carefully to 250 mL borosilicate bottles using tubing to prevent contact with air, preserved with saturated mercuric chloride ($HgCl_2$; 60 μL to 250 mL sample, 120 μL for ice) and stored dark at $+4°C$. In 2012, the sample bottles for the CO_2 system were carefully and quickly opened and reclosed to preserve the samples with $HgCl_2$. For the nutrient samples, the same bottles were used as in 2012.

The pieces of glacial ice were individually placed into plastic bags and put into an insulated box for transportation to lab for further processing. In the laboratory, the glacial ice samples were carefully placed in Tedlar© gas sampling bags and saturated $HgCl_2$ was added (100 μL for 500 mL melted ice) to halt biological activity. After sealing the bags, air was removed from the bag using a vacuum pump. The glacial-ice samples were thawed in darkness at $+4°C$ for 24–48 h resulting in a melted sample of approximately 1 L. The crystals found in the melted glacial ice were sampled with a Nalgene® pipette and placed in 5–10 mL Nalgene® bottles (Thermo Fisher Scientific, USA) with 75% ethanol and stored at $-20°C$.

The temperature of glacial ice and water-column samples was measured on site, immediately after the sample recovery, using a digital probe (Testo 720) with the precision of $\pm 0.1°C$ and accuracy of $\pm 0.1°C$. The holes for the temperature measurement in glacial ice were carefully drilled with a clean stainless steel drill to avoid additional heating from the drill. In addition to sample bottle measurement of temperature and salinity, we obtained hydrography data by deploying conductivity/temperature/pressure (CTD)-probes through the ice hole on stations shown in Table 1. In 2012, we used a STD 204 (SAIV A/S, Norway) with a resolution of ± 0.01 and accuracy of ± 0.02, and in 2013, we used a SBE 37 MicroCAT (Seabird Electronics, USA) with a resolution of ± 0.0001 and accuracy of ± 0.003.

3.2. Analysis

The samples of fjord water and melted glacial ice were analyzed for total alkalinity (A_T), total inorganic carbon (C_T), dissolved inorganic nutrients (nitrate + nitrite, phosphate, and silicic acid), $\delta^{18}O$, and salinity. The salinity of the melted glacial ice and water-column samples was measured using a conductivity meter (WTW Cond 330i, Germany) with a precision and accuracy of ± 0.05.

3.2.1. Determination of the CO_2 System

C_T and A_T were analyzed between 1 day after thawing and within 2 weeks after collection at the laboratory at the Institute of Marine Research, Norway. Analytical methods for C_T and A_T determination in seawater samples are fully described in *Dickson et al*. [2007]. Briefly, C_T was determined using gas extraction of acidified sample followed by coulometric titration and photometric detection using a Versatile Instrument for the Determination of Titration carbonate (VINDTA 3C, Marianda, Germany). The A_T values were determined in the water-column samples from potentiometric titration with 0.1 N hydrochloric acid using a Versatile Instrument for the Determination of Titration Alkalinity (VINDTA 3C, Marianda). The A_T values in melted glacial ice were determined using an automated system for potentiometric titration in an open cell using 0.05

N HCl (Methrohm© Titrando system, Switzerland), as described in *Mattsdotter-Björk et al*. [2014]. The average standard deviation for A_T, determined from replicate sample analyses from one sample, was within ±1 μmol kg^{-1} for water samples. For glacial-ice meltwater, the replicate samples were within ±2 μmol kg^{-1}. The average standard deviation for C_T, determined from replicate sample analyses from one sample, was within ±1 μmol kg^{-1} for all sample varieties. Routine analyses of Certified Reference Materials (CRM, provided by A. G. Dickson, Scripps Institution of Oceanography, USA) ensured the accuracy of the measurements, which was better than ±1 and ±2 μmol kg^{-1} for C_T and A_T, respectively.

We used C_T, A_T, phosphate, silicic acid, salinity, temperature, and depth (pressure) for each sample as input parameters in a CO_2-chemical speciation model (CO2SYS program) [*Pierrot et al*., 2006] to calculate all the other parameters in the CO_2 system such as pH in situ, CO_2 fugacity and partial pressure (fCO_2, pCO_2), carbon dioxide concentration ($[CO_2]$) and carbonate-ion concentration ($[CO_3^{2-}]$), and calcium-carbonate saturation states in the water column (Ω) for aragonite (Ω_{Ar}) and calcite (Ω_{Ca}). We used the total hydrogen-ion scale (pH_T), the HSO_4^- dissociation constant of *Dickson* [1990] and *Mucci* [1983] for the solubility products of aragonite and calcite, and the CO_2 system dissociation constants (K^*_1 and K^*_2) estimated by *Roy et al*. [1993, 1994].

3.2.2. Determination of Dissolved Inorganic Nutrients

The nutrient concentrations of nitrate ($[NO_3^-]$) + nitrite ($[NO_2^-]$), phosphate ($[PO_4^{3-}]$), and silicic acid ($[Si(OH_4)]$) were analyzed in liquid phase in all samples. Colorimetric determinations of nitrate + nitrite and of soluble reactive phosphorus and orthosilicic acid (hereafter abbreviated as nitrate, phosphate, and silicic acid) were performed in triplicate using a Flow Solution IV analyzer (O.I. Analytical, USA) with routine seawater methods adapted from *Grasshoff et al*. [2009]. The Analyzer was calibrated using reference seawater from Ocean Scientific International Ltd., UK, and analytical detection limits (precision) were obtained from six replicate analyses on the same sample. Analytical detection limits were 0.15 μmol kg^{-1} for nitrate, and 0.02 μmol kg^{-1} for phosphate and silicic acid, respectively.

3.2.3. Determination of Oxygen Isotopic Ratios

Stable oxygen isotopic ratios ($\delta^{18}O$) were analyzed using a Picarro L2120-i Isotopic Liquid Water Analyzer with High-Precision Vaporizer AO211 and Thermo Fisher Scientific Delta V Advantage mass spectrometer with Gasbench II. The reason for using different methods was the fact that we used different laboratories for the samples collected in 2012 and 2013. The isotope values using both methods are reported in the common delta notation relative to Vienna Standard Mean Ocean Water (VSMOW) standard. The reproducibility of replicate analysis for the $\delta^{18}O$ measurements was ±0.1‰ for both the Picarro (2012 samples) and for the Gasbench II (2013 samples).

3.2.4. Determination of Mineral Content in Glacial Ice and Bedrock

Mineralogical phase identification was done using a WITec alpha 300 R (WITec GmbH, Germany) confocal Raman microscope. The measurements have been done using an excitation wavelength of 488 nm and an ultra-high throughput spectrometer (UHTS 300, WITec GmbH, Germany) with a grating, 600/mm, 500 nm blaze. The samples were placed in a glass petri dish filled with crushed ice and immediately measured using a water submersible objective (20× Olympus). Raman measurements allow a reliable identification of carbonate and silicate minerals based on their distinct molecular spectra which are related to the inelastic scattering of light [e.g., *Gillet et al*., 1993; *Nehrke and Nouet*, 2011].

3.2.5. Freshwater Fraction Calculation

Freshwater fractions were calculated using the following equation (1):

$$\text{Freshwater fraction} = 1 - S_{meas}/S_{ref} \quad (1)$$

where S_{ref} is the mean salinity of the transformed Atlantic water (winter water) of 34.9 ± 0.06, measured in the water column in April 2013. S_{ref} is also within the salinity range (34.7–34.96) of the transformed Atlantic water reported by *Svendsen et al*. [2002]. S_{meas} is the measured salinity in the water samples.

4. Results and Discussion

4.1. Spatial and Interannual Variability of Fjord Hydrography

In March/April 2012, the salinity (Figure 2a) and temperature (Figure 2b) showed a clear change from fresher and colder water in the upper 15 m close to the glacier to more saline and warmer waters in the outer parts of the fjord. In March 2012, the salinity varied between 28.3 and 34.3 in the upper 20 m and in

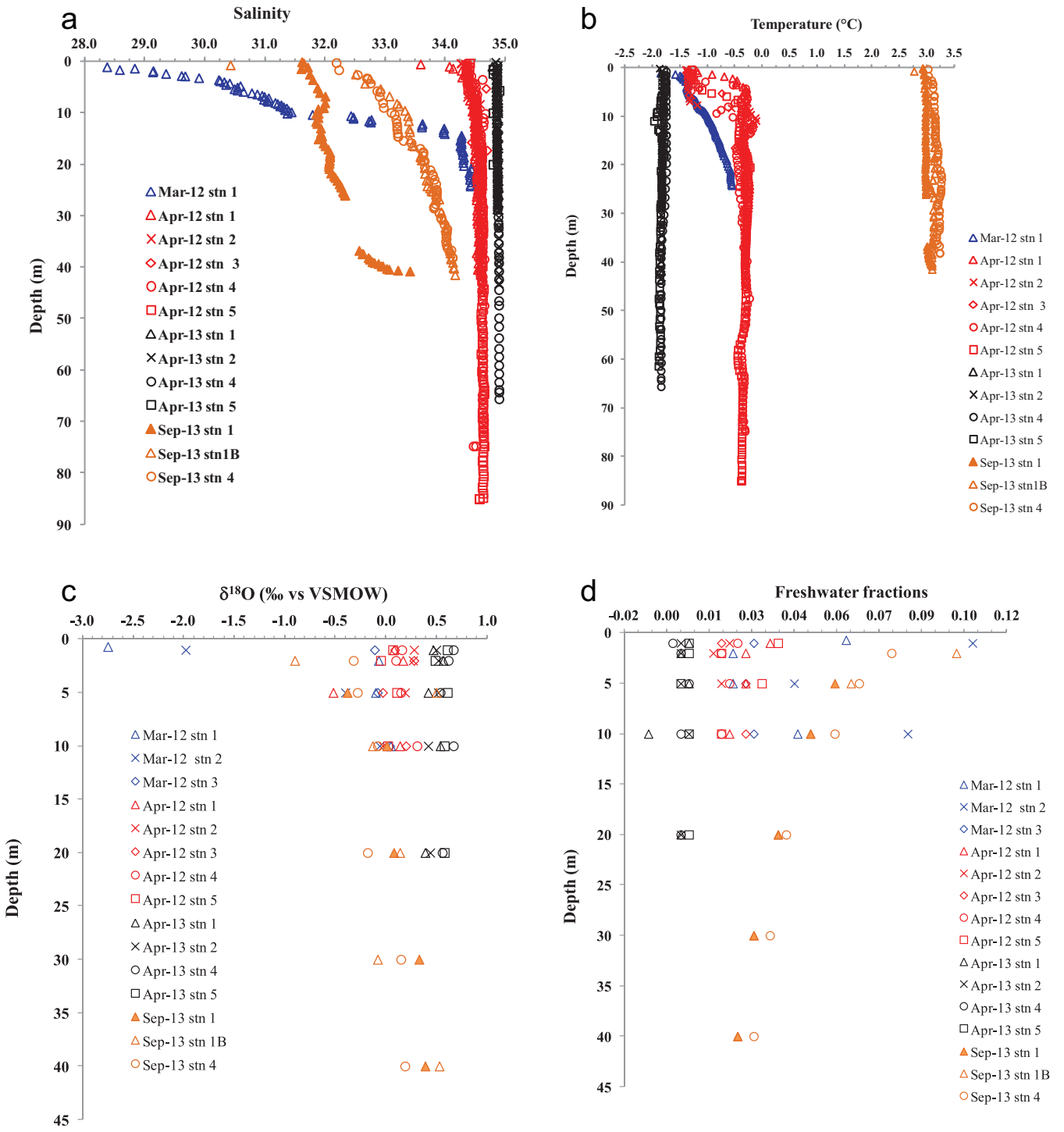

Figure 2. Vertical profiles of seawater (a) salinity, (b) temperature (°C), (c) oxygen isotopic ratio ($\delta^{18}O$ ‰ versus VSMOW), and (d) freshwater fractions during March 2012 (blue open symbol), April 2012 (red open symbols), April 2013 (black filled symbols), and September 2013 (orange symbols) in Tempelfjorden.

April 2012 between 33.6 and 34.7 (Figure 2a). From March to April 2012, the minimum salinity had increased from 28.3 to 33.6 in the upper 2–5 m. At that time, the temperature varied from −1.6 to −0.3°C and the top 10 m had warmed up to 1°C in 1 month (from March to April 2012) creating a thermocline at about 10 m depth at the fjord mouth and shallower at the glacier front (Figure 2b). These stratified conditions were in strong contrast to the conditions in April 2013, where there was a well-mixed layer with homogeneous

Table 2. Physical and Chemical Properties of Glacial Ice Sampled at Station Next to the Glacier Front of von Postbreen[a]

Date		Stn	T (°C)	S	A_T (μmol kg^{-1})	C_T (μmol kg^{-1})	[NO_3^-] (μmol kg^{-1})	[PO_4^{3-}] (μmol kg^{-1})	[$Si(OH)_4$] (μmol kg^{-1})	$\delta^{18}O$ (‰ Versus VSMOW)	N
11 Apr 2012	Median	1	−5	n/a	n/a	n/a	0.2	0.03	1.60	−13.6	3
	Stdev			n/a	n/a	n/a	1.5	<0.02	1.29	2.9	3
	Min			0.0	n/a	n/a	0.1	0.02	0.02	−16	3
	Max			0.4	177	102	3.9	0.03	3.17	−9.8	3
12 Apr 2013	Median	1	−6	0.0	0	21	0.2	0.05	0.00	−15.4	3
	Stdev			0.0	0	8	0.2	0.03	0.00	0.3	3
	Min			0.0	0	9	<0.2	<0.02	0.00	−15.7	3
	Max			0.0	0	23	0.4	0.06	0.00	−15.0	3
18 Sep 2013	Median	1	0.1	0.0	140	137	<0.2	<0.02	0.00	n/a	6
	Stdev			0.0	136	53	<0.2	<0.02	0.00	n/a	6
	Min			0.0	68	89	<0.2	<0.02	0.00	n/a	6
	Max			0.0	378	194	<0.2	<0.02	0.00	n/a	6

[a]T denotes temperature, S refers to salinity, and N means number of samples. n/a means not applicable.

salinity of about 34.9, and cold water just above freezing point from top to bottom. There was no water-column stratification and no discernible spatial gradient from the glacier front to the outer fjord in April 2013 (Figures 2a and 2b). Overall, the water column below 10 m was more than 1°C colder in April 2013 than in April 2012. The cold water at near freezing temperatures in April 2013, combined with a constant and high salinity (>34.9) throughout the water column, indicated the influence of winter water. The presence of winter water was confirmed by the relatively high $\delta^{18}O$ values (Figure 2c) and zero freshwater fractions (Figure 2d) in April 2013. The $\delta^{18}O$ values were homogeneously distributed with a mean value and standard deviation for all samples of 0.55 ± 0.07. In winter 2012, the $\delta^{18}O$ values were lower than in winter 2013 and showed larger $\delta^{18}O$ variability, indicated by the mean value and standard deviation of −0.11 ± 0.6. The values near the glacier were mostly negative with a minimum value of −2.8‰ (Figure 2c). Low $\delta^{18}O$

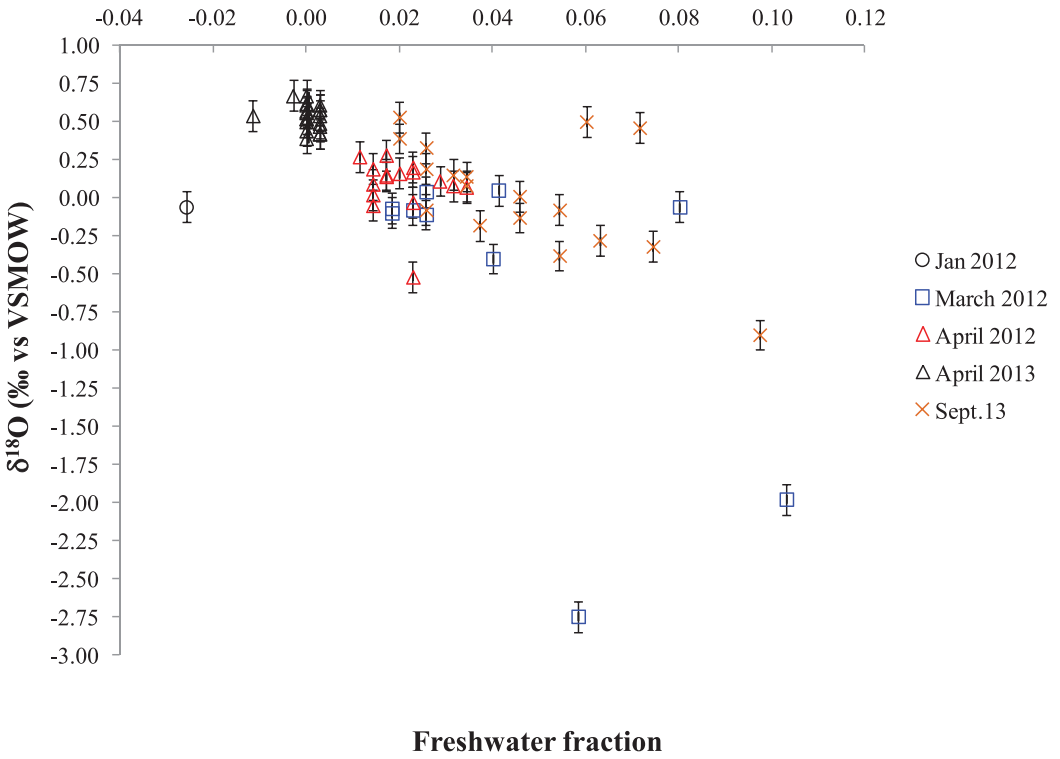

Figure 3. Oxygen isotopic ratio ($\delta^{18}O$ ‰ VSMOW) versus freshwater fractions in January 2012 (open black circles), March 2012 (open blue squares), April 2012 (open red triangles), April 2013 (open black triangles), and September 2013 (orange crosses). The vertical error bars show the error introduced by the analytical precision for $\delta^{18}O$ of ±0.1‰.

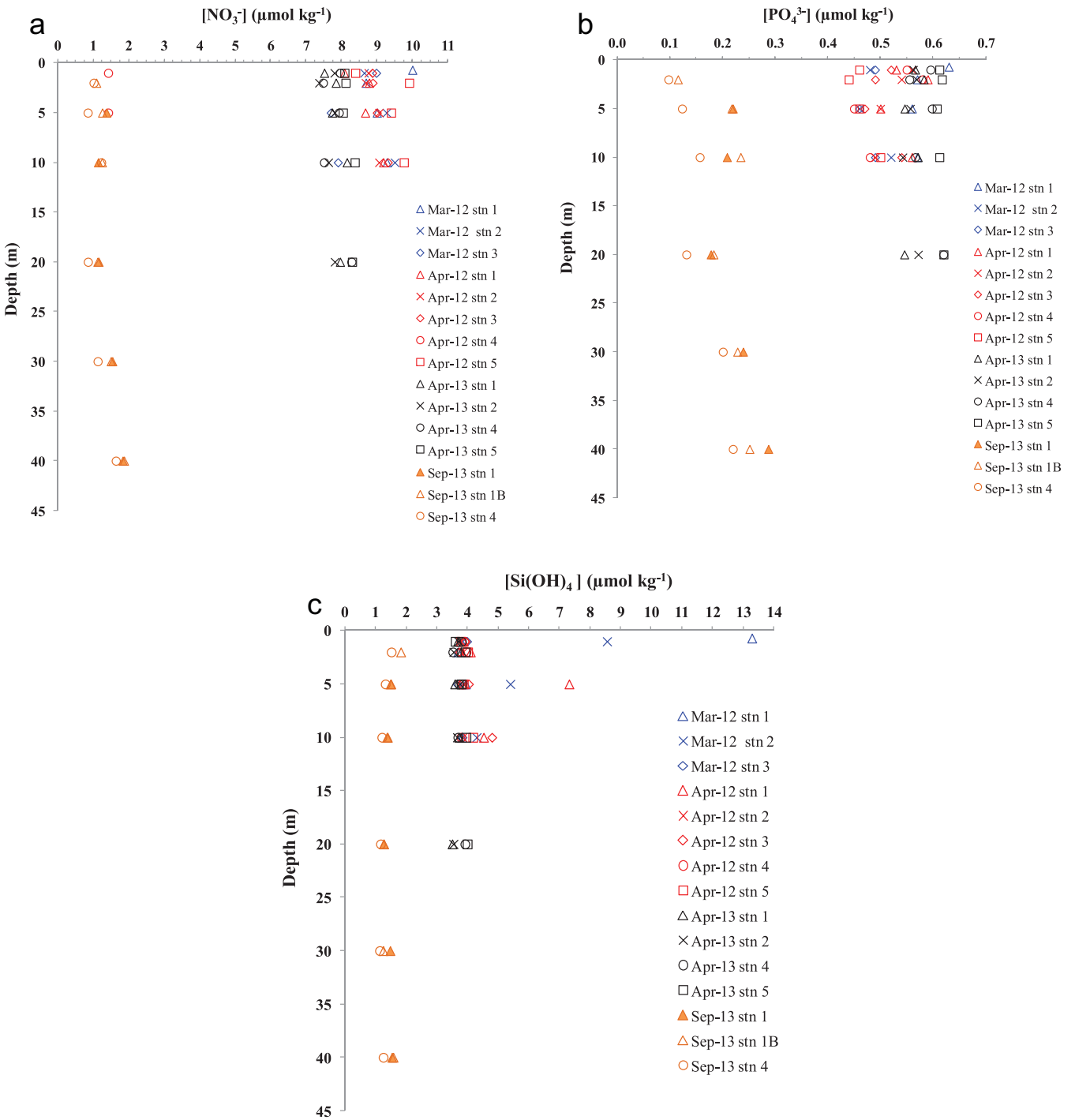

Figure 4. Vertical profiles of seawater concentrations (μmol kg^{-1}) of (a) nitrate ([NO_3^-]), (b) phosphate ([PO_4^{3-}]), and (c) silicic acid ([$Si(OH)_4$]) during March 2012 (blue symbols), April 2012 (red symbols), April 2013 (black symbols), and September 2013 (orange symbols) in Tempelfjorden.

values indicate freshwater influence from glacier melt which was also noted by the relatively high freshwater fractions varying between 0.01 and 0.11 in winter 2012 (Figure 2d).

The water temperature in September was a result of summer warming of approximately 5°C in the top 10 m from April to September 2013 (Figure 2b). In summer (September 2013), salinity and $\delta^{18}O$ were lower than during the winter months, reflecting more freshwater supply of glacial drainage water in summer, as

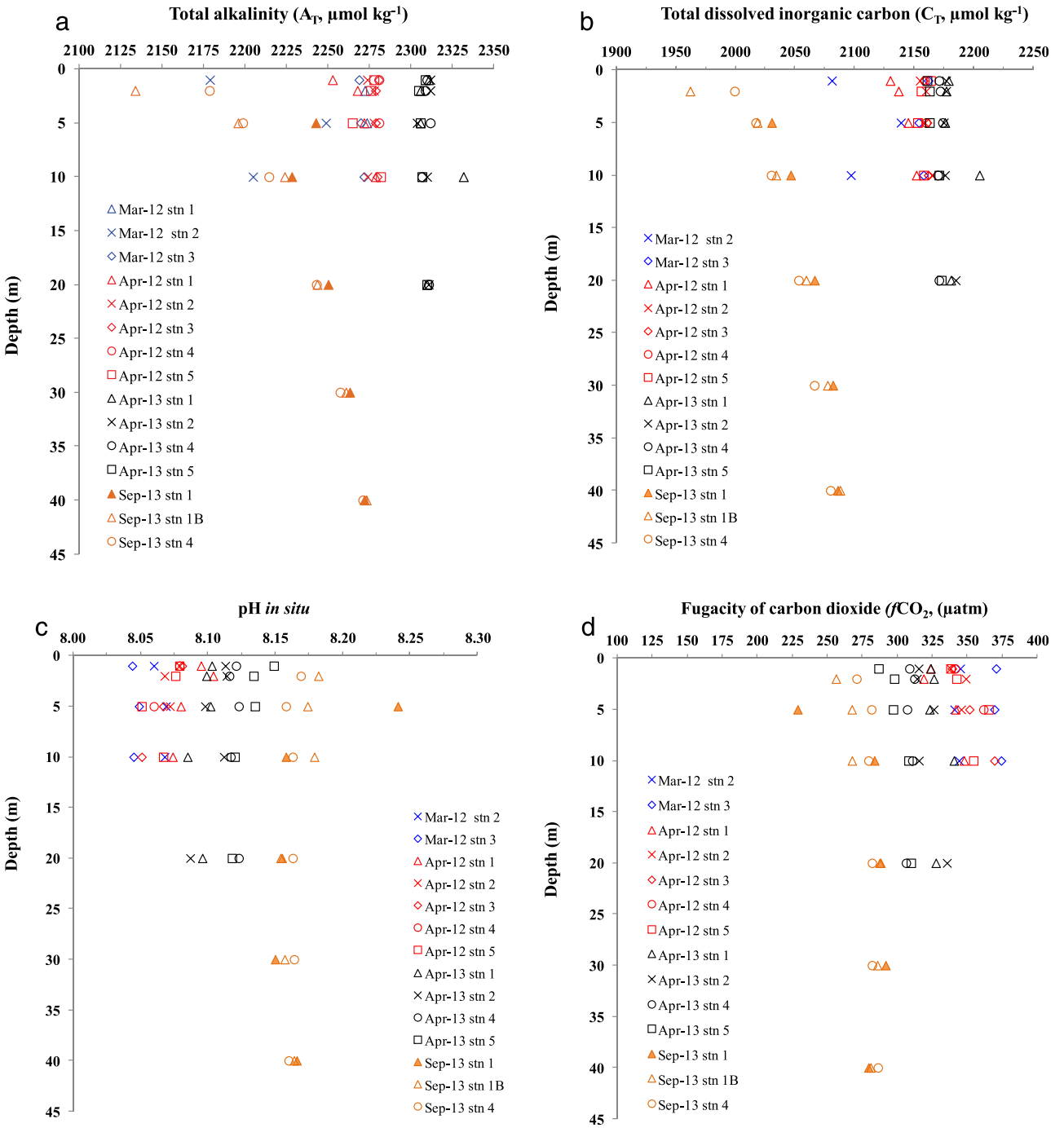

Figure 5. Vertical profiles of seawater (a) total alkalinity (A_T, μmol kg^{-1}), (b) total inorganic carbon (C_T μmol kg^{-1}), (c) in situ pH, (d) fugacity of CO_2 (fCO_2, μatm), (e) calcium carbonate saturation state of aragonite (Ω_{Ar}), and (f) calcium carbonate saturation state of calcite (Ω_{Ca}) during March 2012 (blue symbols), April 2012 (red symbols), April 2013 (black symbols), and September 2013 (orange symbols) in Tempelfjorden.

almost all freshwater supplies usually occur from June to August [*Nilsen et al.*, 2008]. This was observed in the relative higher freshwater fractions (Figure 2d). The $\delta^{18}O$ values were negative in the surface waters (<5 m) and close to zero deeper down in the water column.

The glacial ice in our study had a minimum $\delta^{18}O$ value of $-16‰$ (Table 2), in close agreement with the glacial ice in Kongsfjorden area which had a mean $\delta^{18}O$ value of $-15.85‰$ [*MacLachlan et al.*, 2007]. The slope

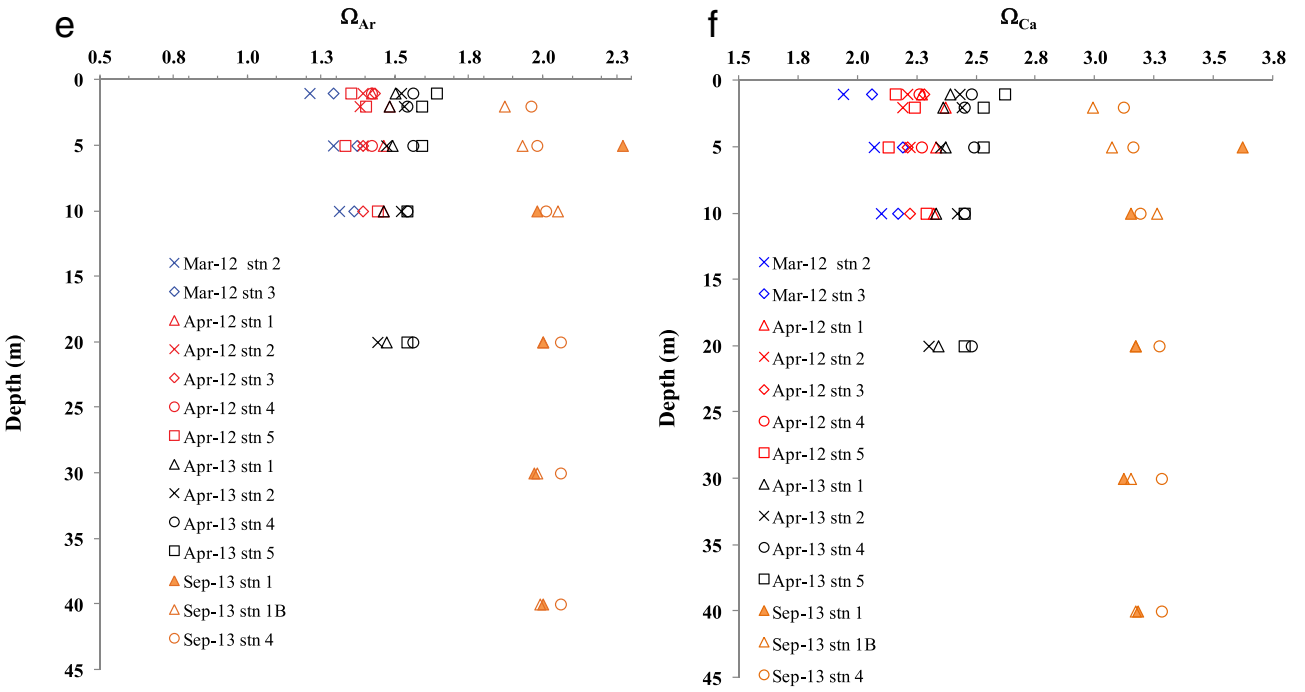

Figure 5. (continued).

of the regression (not shown) between mean values of $\delta^{18}O$ versus salinity of seawater (N = 68) and glacial ice (N = 12) was 0.44, which was similar to what was found in Kongsfjorden by *MacLachlan et al.* [2007]. This agreement indicates that there were similar water masses in Tempelfjorden and Kongsfjorden. Figure 3 shows that the $\delta^{18}O$ values generally decrease with increased freshwater fractions.

4.2. Spatial and Interannual Variability of Nutrients in the Fjord

In April 2012, $[NO_3^-]$ increased by 0.07 μmol kg^{-1} km^{-1} from glacier front to the outer fjord at 5 m depth (Figure 4a). The $[PO_4^{3-}]$ was almost constant along the fjord and showed only a small decrease of about 0.01 μmol kg^{-1} km^{-1} (Figure 4b). The $[Si(OH)_4]$ was nearly constant at about 4 μmol kg^{-1}, except for the almost twice as high levels at the glacier front (Figure 4c). Along-fjord gradients at 5 m depth in April 2013 showed increasing levels on all three nutrients from the glacier front to the outer fjord of 0.04, 0.09, and 0.02 μmol kg^{-1} km^{-1} for $[NO_3^-]$, $[PO_4^{3-}]$, and $[Si(OH)_4]$, respectively. Interannual variability in winter showed that the $[NO_3^-]$ concentrations (Figure 4a) were higher in April 2012 than in April 2013, and $[PO_4^{3-}]$ (Figure 4b) was lower in April 2012 than in April 2013. The $[Si(OH)_4]$ concentrations (Figure 4c) in March and April 2012 differed significantly at the stations near the glacier compared to the outer fjord, where higher $[Si(OH)_4]$ were recorded in March/April 2012 than in April 2013 in the top 10 m. This may indicate the addition of $[Si(OH)_4]$ from dissolved silicate-rich bedrock at the glacier, which is similar to that observed by *Azetsu-Scott and Syvitski* [1999] in a western Greenland fjord. They observed elevated $[Si(OH)_4]$ near the glacier.

Between April 2013 and September 2013, all three nutrients showed a large decrease. The $[NO_3^-]$ levels decreased eight times and $[PO_4^{3-}]$ six times relative to the April 2013 levels. In September 2013 $[NO_3^-]$ and $[PO_4^{3-}]$ values were below detection limit (Figures 4a and 4b).

4.3. Spatial and Interannual Variability of the CO_2 System and OA State in the Fjord

In 2012, the lowest A_T and C_T were observed at the stations near the glacier (stations 1 and 2, Figure 1), particularly in March 2012 (Figures 5a and 5b) where the lowest A_T of 2180 μmol kg^{-1} was observed. Along-fjord gradients at 5 m depth in April 2012 showed an A_T increase of approximately 1.5 μmol kg^{-1} km^{-1} from inner to outer parts of the fjord. All A_T and C_T values were about 40 μmol kg^{-1} lower in April 2012 than in April 2013. This resulted in the lowest in situ pH in winter 2012 (Figure 5c). The lower A_T in winter 2012 coincided with lower salinities this winter (Figure 2a) and higher freshwater fractions (Figure 2d). In April 2013, A_T and C_T showed no gradient from the glacier to the outer fjord stations and were almost

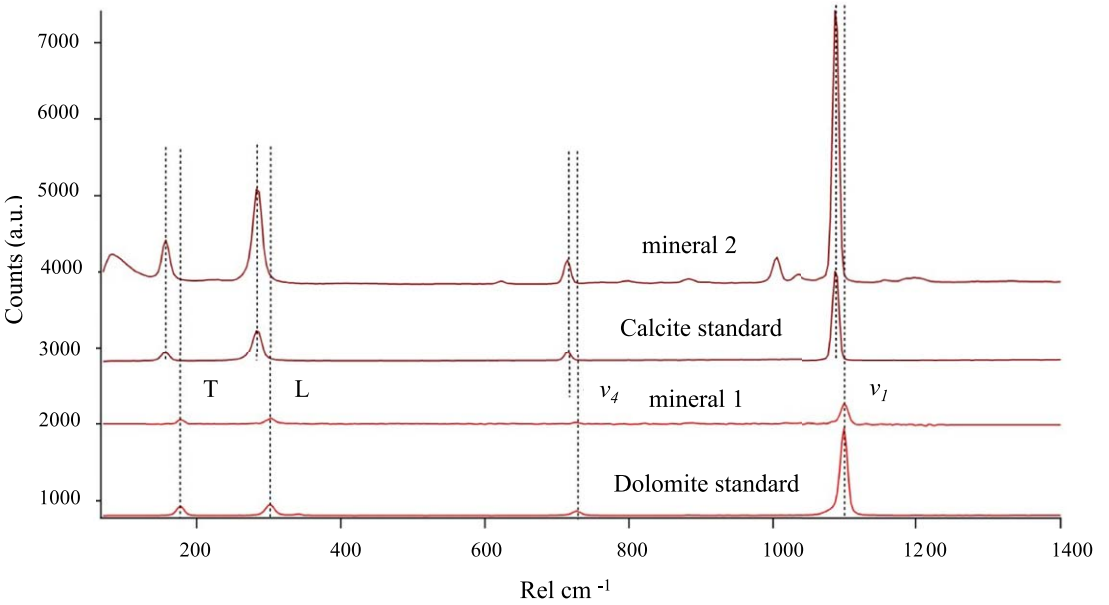

Figure 6. Raman spectra of dolomite, calcite, and two minerals (#1 and #2) from the glacial ice sample. It can be seen that the spectral position (given in relative wavenumbers; rel. cm^{-1}) of two lattice modes (translation mode; T and librational mode; T) as well as the two internal modes (in-plane band; $\nu 4$ and symmetric stretch $\nu 1$) unambiguous proved the presence of dolomite and calcite in the investigated sample.

constant in the upper 20 m. This was indicated by the truncated mean values and low standard deviations of 2309 ± 3 μmol kg^{-1} for A_T and 2173 ± 6 μmol kg^{-1} for C_T (Figures 5a and 5b). By September 2013, A_T had decreased by approximately 135 μmol kg^{-1} and C_T by approximately 100 μmol kg^{-1} from April (Figures 5a and 5b).

In March/April 2012, in situ pH was generally lower and fCO_2 higher compared to the values in April 2013 (Figures 5c and 5d). Spatial gradients of in situ pH and fCO_2 from the near glacier front to the outer fjord showed significant and opposing gradients between the two winters. In April 2012, the in situ pH decreased by 0.0036 units km^{-1} coinciding with a fCO_2 increase of 3 μatm km^{-1}. This was in contrast to the situation in April 2013 where in situ pH increased by 0.0045 units km^{-1} and fCO_2 decreased by 3.6 μatm km^{-1} from the glacier front to the outer fjord.

At all times, seawater fCO_2 was undersaturated relative to the atmospheric fCO_2 (of approximately 400 μatm, Ny-Ålesund station, Spitsbergen) (Figure 5d) and varied between 250 μatm (September 2013) and 370 μatm (March 2012). In September 2013, we observed the highest in situ pH and lowest fCO_2 (Figures 5c and 5d).

The lowest Ω_{Ar} and Ω_{Ca} were found in March and April 2012 (Figures 5e and 5f) and the Ω_{Ar} values decreased by approximately 0.012 km^{-1} from the inner to the outer fjord. In April 2013, Ω was >1 (Ω_{Ar}, Figure 5e; Ω_{Ca}, Figure 5f). The lowest values were found near the glacier front and higher values further out in the fjord, with a difference ($\Delta\Omega_{Ar}$) of approximately 0.2 (increasing from the glacier front to outer fjord by 0.015 km^{-1}).

4.4. Chemical Properties and Mineral Composition of Glacial Ice

The melted glacial ice contained significant [NO_3^-] and [$Si(OH)_4$] in winter, with the maximum [NO_3^-] of 3.9 μmol kg^{-1} and [$Si(OH)_4$] of 3.17 μmol kg^{-1} in April 2012 (Table 2). The [PO_4^{3-}] values were low and ranged between 0.01 and 0.06 μmol kg^{-1}. The [$Si(OH)_4$] was below detection limit in April 2013, and all three nutrients were below detection limit in September 2013 (Table 2). This month we found that the melted glacial ice contained relatively high A_T and C_T values of 378 and 194 μmol kg^{-1}, respectively (Table 2). These maximum values resulted in the highest [CO_3^{2-}] of 154 μmol kg^{-1} which was higher than the mean seawater [CO_3^{2-}] (all samples) of 109 ±20 μmol kg^{-1}. The high [CO_3^{2-}] in these samples could be caused by calcareous minerals. The presence of dolomite (mineral 1) and calcite (mineral 2) crystals incorporated in glacial ice was confirmed by confocal Raman microscopy (Figure 6). The spectral position of two lattice modes as well as the two internal modes of dolomite and calcite, respectively, matched exactly the ones

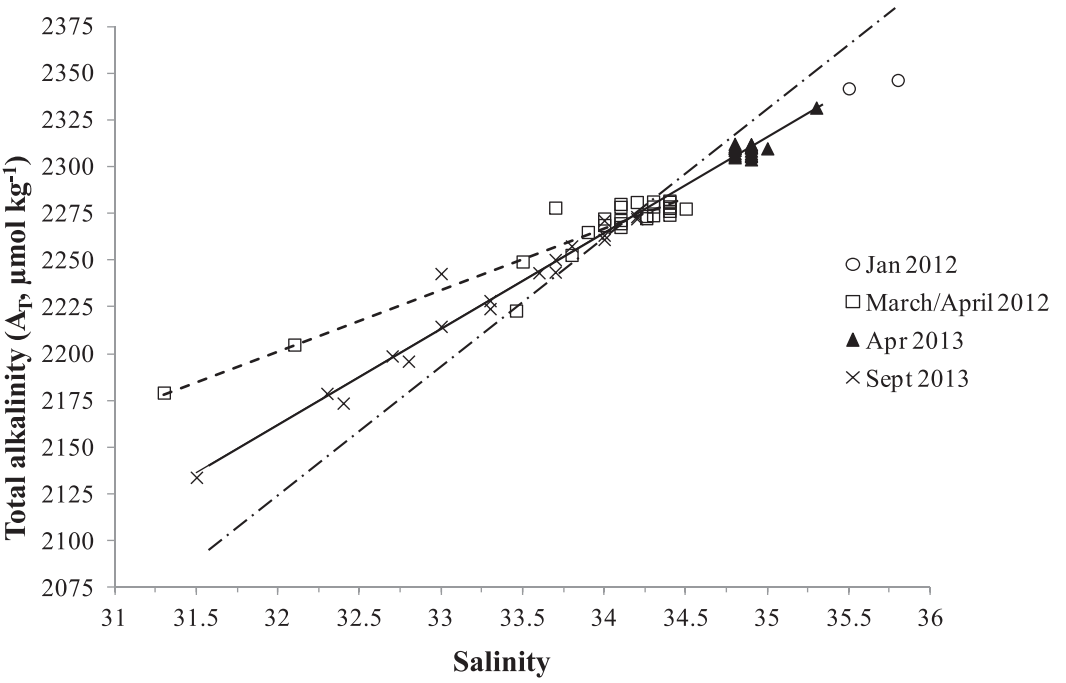

Figure 7. Linear relationship between salinity (*x* axis) and total alkalinity (A_T, μmol kg^{-1}, *y* axis) during January 2012 (open circles), March and April 2012 (open squares), April 2013 (filled triangles), and September 2013 (crosses). The linear relationships were for: winter 2012 (March and April 2012) $A_T = 33.08x + 1142$, $R^2 = 0.901$, dashed line; for all values in 2013 (April 2013 and September 2013), $A_T = 51.13x + 526$, $R^2 = 0.984$, black line. The intercept of the linear relationship at zero-salinity based on 2013 values was A_T =66.54, $R^2 = 0.895$, dashed dotted line.

determined for the two minerals. In the melted glacial ice samples, we also found quartz (SiO_2, not shown), which could explain the relatively high [$Si(OH)_4$] in the glacial ice and in the water near the glacier front.

4.5. Effect of Glacial Drainage Water on Chemistry and Ocean Acidification State

Depending on the mineralogy of the drainage basin, the freshwater from glacial melt and drainage from glacier basins (e.g., land-derived water) have the potential to affect water-column chemistry, air-sea CO_2 flux, and ocean acidification (OA state) in several ways. Direct input of glacial water from marine terminating glaciers (melting of calving icebergs and surface melt) adds freshwater which is much less affected by chemical components from the bedrock, compared to runoff derived from the glacial drainage basin (indirect input). Here at the base of the glacier, chemical components are accumulated and added to the water due to erosion from the bedrock through glacier-water action (friction and lubrication) [*Benn et al*., 2007]. Consequently, the composition of the bedrock minerals has the potential to affect the buffer capacity (carbonate system and A_T) and OA state in the receiving water body. Our data clearly show that the chemistry and OA state in the fjord water were affected by differences in freshwater fraction and the result of sea-ice condition (e.g., ice cover and haline convection). Interestingly, the linear relation between A_T and salinity indicated two different freshwater end-members (at zero salinity); one with A_T of 1142 μmol kg^{-1} based on March and April 2012, and one end-member with lower A_T of 526 μmol kg^{-1}, where most of the September 2013 values were aligned (Figure 7). This indicated that the freshwater source in winter 2012 was more influenced by indirectly derived carbonate ions from the glacial drainage basin resulting in higher A_T at zero-salinity compared to in September 2013. A minor part of the A_T increase could also be due to the supply of dissolved silicate-rich bedrock, contributing to A_T. In September, the water was likely more influenced by direct freshwater supply and was closer to the dilution line with pure water (dot-dashed line, Figure 7). The slope for the A_T-salinity relationship is 33 μmol kg^{-1} A_T per unit salinity for the March and April 2012 data, whereas it is 51 μmol kg^{-1} per unit salinity for the April and September 2013 data (Figure 7). The corresponding slope for the dilution of pure water was 66 μmol kg^{-1} per unit salinity. This implies that in winters, similar to March 2012 with a large amount of glacial drainage water, the fjords will receive freshwater with a larger buffer capacity than freshwater derived from the direct surface freshwater addition. At a few occasions (January 2012 and April 2013), the salinity was higher than 34.9 and A_T was below the dilution

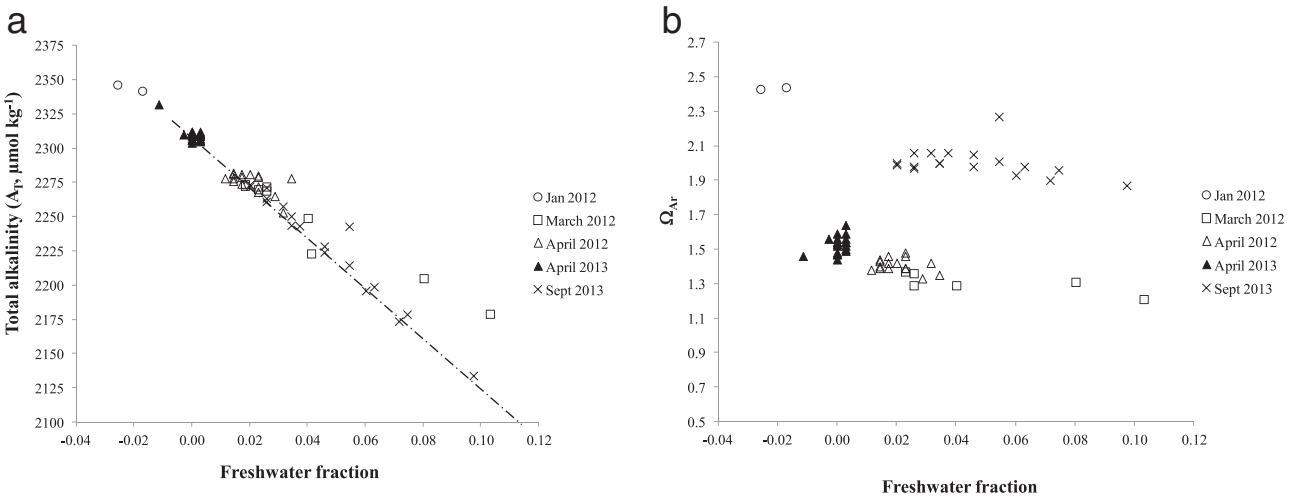

Figure 8. Freshwater fractions (*x* axis) versus (a) total alkalinity (A_T, μmol kg^{-1}), and (b) aragonite saturation state (Ω_{Ar}) in January 2012 (open circles), March 2012 (open squares), April 2012 (open triangles), April 2013 (filled triangles), and September 2013 (crosses). The dashed dotted line in Figure 7a shows the dilution for the April 2013 data.

line (Figure 7). This deviation suggests a rejection of A_T-depleted brine from the sea ice due to $CaCO_3$ precipitation within the sea ice, leaving excess A_T (as $CaCO_3$) in the sea ice [e.g., *Rysgaard et al*., 2007; *Fransson et al*., 2013].

Although, higher A_T in the freshwater end-members results in higher capacity to buffer against acidic input, our results showed decreasing A_T and Ω with increasing freshwater fractions (Figures 8a and 8b). Most of the data points in March and April 2012 are higher than the dilution line (Figure 8a). The drainage basin near the glacier was influenced by freshwater draining into bedrock containing carbonate ions ($[CO_3^{2-}]$) [*Dallmann et al*., 2002; *Forwick et al*., 2010]. In our study, we found evidence for dolomite and calcite in the glacial ice. A detailed study of the mineral composition in the drainage waters by *Forwick et al*. [2010] reported that the waters emanating from Tunabreen and von Postbreen contained sediments that consisted of about 30% dolomite ($CaMg(CO_3)_2$), ankerite ($Ca(Fe, Mg, Mn)(CO_3)_2$, and 18% calcite ($CaCO_3$), all of which can contribute with carbonate ($[CO_3^{2-}]$), magnesium ($[Mg^{2+}]$), and calcium ions ($[Ca^{2+}]$). In the study area, the drainage water also contained dissolved minerals from silicate-rich bedrock that also contributes with $[Mg^{2+}]$ and calcium ions $[Ca^{2+}]$. This means that these glaciers and drainage water have the potential to affect the CO_2 system, Ω, and the air-sea CO_2 flux. Dissolved silicate-rich bedrock, such as silicate and magnesium hydroxide ($MgOH^+$) also contributes to A_T but has a minor impact in seawater (0.2% and 0.1%, respectively) in comparison to the impact of $[CO_3^{2-}]$ supply (6.7%) [e.g., *Millero*, 2013]. The contribution of $[Ca^{2+}]$ from Arctic river discharge has shown to increase ocean Ω_{Ar} although dilution due to freshening [*Azetsu-Scott et al*., 2010]. Our study strengthens the previous results that showed that increased freshwater results in decreased Ω (and gives a positive feedback on OA). However, it also shows that glacial runoff from drainage basins containing carbonate and silicate-rich bedrock has the potential to alleviate OA and Ω to some extent. Similar results of decreased pH and Ω due to the effect of glacial drainage water were found in the sub-Arctic inland sea of the Prince William Sound in Alaska by *Evans et al*. [2014].

4.6. Biological CO_2 Uptake and Air-Sea CO_2 Exchange

Glacier fronts are known to induce primary production and hence secondary production due to upwelling of nutrient and mineral-rich water as a result of plumes of water from the glacier entering the fjord [e.g., *Apollonio*, 1973; *Lydersen et al*., 2014]. Here we estimate the biological CO_2 uptake of the surface water at the glacier front (stn #1) and near the sea ice edge (stn #4) using changes in C_T, $[NO_3^-]$, and A_T between April 2013 and September 2013. The values were corrected for freshwater dilution (C_{corr}) based on freshwater fractions in the surface water in September (f and $f_{ww} = 1 - f_{glac}$) and the mean values of the end-member concentrations (C) of $[NO_3^-]$, C_T, and A_T in the glacial drainage water (C_{glac}) and in the surface winter water (C_{ww}; Table 3). The end-member concentration of C_T is assumed to be the same as A_T [*Fransson et al*., 2001]. The corrected values were subtracted from the observed (C_{obs}) September values for stns 1

Table 3. Properties of Source Waters of Winter Water (ww) From April 2013 Data and Glacial Drainage Water (glac), and Surface Water (2 m depth) Values in September 2013 at Stations #1 (C_{obs}#1) and #4 (C_{obs}#4), and Values Corrected for Freshwater Dilution (C_{corr}) Based on the Fractions of Winter Water (f_{ww}) and Freshwater Fractions (f_{glac}) in Surface Water at Stations #1 and #4 in September[a]

	ww	glac	C_{obs} #1	C_{obs} #4	C_{corr} #1	C_{corr} #4
S	34.9 ± 0.06	0	31.5 ± 0.01	32.2 ± 0.01	n/a	n/a
C_T (μmol kg^{-1})	2173 ± 5	526 ± 3	1964 ± 1	2000 ± 1	2008 ± 16	2041 ± 16
NO_3 (μmol kg^{-1})	8.3 ± 0.29	0.8 ± 0.15	1.1 ± 0.15	1.1 ± 0.15	7.55 ± 0.08	7.7 ± 0.08
A_T (μmol kg^{-1})	2309 ± 2	526 ± 3	2134 ± 1	2179 ± 1	2131 ± 18	2166 ± 18
fx #1	0.90 ± 0.01	0.10 ± 0.01	n/a	n/a	n/a	n/a
fx #4	0.92 ± 0.01	0.08 ± 0.01	n/a	n/a	n/a	n/a

[a]Standard deviation denotes the cumulative error based on the analytical precision and the natural variability of the input parameters and the propagated error in C_{corr}.

and #4 at the depth of the largest change (i.e., top 2 m; Table 3) in order to calculate changes (ΔC) due to processes other than freshwater dilution such as biological carbon uptake and air-sea CO_2 exchange according to the equations (2) and (3):

$$C_{corr} = C_{glac} \times f_{glac} + C_{ww} \times f_{ww} \quad (2)$$

$$\Delta C = C_{obs} - C_{corr} \quad (3)$$

The carbon loss due to biological CO_2 uptake (C_{bio}) was obtained from the $\Delta[NO_3^-]$ converted to carbon equivalents using the carbon:nitrate (C:N) stoichiometric ratio of 106:16 [*Redfield et al*., 1963] (Table 4):

$$C_{bio} = \Delta[NO_3] \times 6.625 \quad (4)$$

We estimated a carbon loss due to C_{bio} of 43 and 44 μmol kg^{-1} for stns #1 and #4, respectively (Table 4). The carbon loss due to ΔC_T (45 and 41 μmol kg^{-1} for stns #1 and #4, respectively) was similar to C_{bio}, which means that biological carbon uptake dominated the change in carbon. Consequently, there was an insignificant exchange of carbon with the surrounding environment such as ocean CO_2 exchange with the atmosphere or contribution from other sources (C_{exch}, equation (5)):

$$C_{exch} = \Delta C_T - C_{bio} \quad (5)$$

Positive C_{exch} indicates a gain due to either ocean uptake of atmospheric CO_2 (C_{atm}) or supply of $[CO_3^{2-}]$ from glacial drainage water (C_{CO32-}, equation (6)):

$$C_{atm} + C_{CO32-} = \Delta C_T - C_{bio} \quad (6)$$

The A_T values are not directly affected by ocean uptake of atmospheric CO_2 and to a minor extent by primary production (PP). By the assimilation of NO_3^- and hydrogen ions for the formation of protein during photosynthesis, the A_T values increase. Consequently, the influence of PP on A_T is similar to $\Delta[NO_3^-]$ (Table 4). The effect on A_T due to primary production (A_{T-PP}, Table 4) can be corrected:

$$A_{T\text{-}PP} = A_{Tcorr} - \Delta[NO_3^-] \quad (7)$$

In order to estimate the effect on A_T and C_T of the mineral supply from the dissolution of carbonate-rich bedrock, we used the ΔA_{T-PP} values (Table 4). A gain of $[CO_3^{2-}]$ affects A_T by a factor of two and C_T by one. Hence, the C_T gain due to $[CO_3^{2-}]$ supply (C_{CO32-}) and due to atmospheric CO_2 uptake (C_{atm}) were estimated according to the equations (8) and (9):

Table 4. Summary of the Change of C_T (ΔC_T) and $[NO_3^-]$ (ΔNO_3) and the Biological CO_2 Uptake (C_{bio}), Contribution of Carbonate Ions From Glacial Drainage Water (C_{CO32-}) Estimated From the Change of A_T (ΔA_T) and the A_T Corrected for the Change During Primary Production (ΔA_{T-PP}), and the Contribution From the Uptake of Atmospheric CO_2 (C_{atm})[a]

Stn#	ΔC_T	$\Delta[NO_3]$	C_{bio}	C_{exch}	ΔA_T	ΔA_{T-PP}	C_{CO32-}	C_{atm}
1	−45 ± 17	−6.5 ± 0.3	−43 ± 2	−2 ± 17	+3 ± 18 (ns)	−3 ± 18 (ns)	−1 ± 18 (ns)	0 ± 25
4	−41 ± 17	−6.6 ± 0.3	−44 ± 2	+3 ± 17	+13 ± 18	+6 ± 18	+3 ± 18	0 ± 25

[a]Model calculations for each term are given in equations (1–9). All terms are in μmol C kg^{-1} and negative sign denotes a loss of C_T and positive a gain of C_T. Standard deviation denotes the cumulative error based on the analytical precision and the natural variability of the input parameters and the propagated error in the model parameters.

$$C_{CO32-} = A_{T\text{-}PP} \times 0.5 \quad (8)$$

$$C_{atm} = \Delta C_T - C_{bio} - C_{CO32-} \quad (9)$$

Our estimates of C_{exch}, C_{CO32-}, and C_{atm} based on 2013 data were mainly insignificant, which was partly due to the lower freshwater supply in April 2013 compared to in April 2012. The relatively large total error of ± 25 μmol kg^{-1} in C_{atm} (Table 4) was based on the cumulative uncertainty of the analytical precision and natural variability of the input parameters (Table 3) in the model, and the propagated error in the calculated model parameters. The contribution of the uncertainty of the estimates of freshwater fractions was ± 0.01 based on the cumulative uncertainty in salinity derived from the analytical resolution of ± 0.01 and the variability of salinity in the water column of ± 0.06 in April 2013. Based on this value, we performed a sensitivity check on the resulting C_{exch} and C_{atm} by changing the f_{glac} and f_{ww} of ± 0.01 in the mass-balance model calculations. This exercise showed that decreased freshwater supply resulted in a CO_2 loss of about 18 and 7 μmol kg^{-1} based on C_{exch} and C_{atm}, respectively. Increased freshwater resulted in a CO_2 gain of 14 μmol kg^{-1} (C_{exch}) and 7 μmol kg^{-1}, when accounting for the contribution of carbonate ions (C_{atm}). This also demonstrates that the cumulative uncertainty in the freshwater fraction calculation contributes with ± 7 μmol kg^{-1} of the propagated error of ± 25 μmol kg^{-1} (Table 4). The uncertainty originated from the freshwater fraction calculation becomes smaller with the higher freshwater end-member of 1142 μmol kg^{-1} such as in March–April 2012 (Figure 7).

By assuming a surface mixing of the upper 20 m and the minimum and maximum C_{atm} of -32 to $+32$ μmol kg^{-1}, the estimated oceanic CO_2 source and sink were 0.6 mol C m^{-2}, respectively, for the whole period (April to September) and 0.11 mol C m^{-2} month^{-1} (1.3 gC m^{-2} month^{-1}). The annual exchange was 0.8 mol C m^{-2} yr^{-1} (9 gC m^{-2} yr^{-1}) based on 7 months of open water. Our estimates of the CO_2 sink is lower than the estimates of the average annual sink of atmospheric CO_2 of 2.7 mol C m^{-2} yr^{-1} (or 32 g C m^{-2} yr^{-1}), corresponding to 29 mmol C m^{-2} d^{-1}, in Young Sound, NE Greenland based on an open water period of 9 months [*Sejr et al*., 2011]. However, they used another methodology based on direct surface fCO_2 measurements and flux calculations. For comparison, we performed a similar calculation based on the observed surface fCO_2 values near the glacier in September. Here we found an undersaturation of 144 μatm (402–258 μatm) relative to the atmospheric level of 402 μatm (Ny-Ålesund) implying that the fjord had the potential to act as a sink of atmospheric CO_2 during the open water season, until the onset of ice formation. We calculated the CO_2 flux using the formulation of *Wanninkhof et al*. [1992] in combination with the fCO_2 undersaturation of 144 μatm in September, mean wind speed of 12 m s^{-1}, and the surface-water temperature of 3.2°C. This resulted in an atmospheric CO_2 uptake of 0.35 mol C m^{-2} month^{-1} (12 mmol C m^{-2} d^{-1}) and an annual net sink of 2.5 mol C m^{-2} during 7 months of open water, which is similar to the annual sink of 2.7 mol C m^{-2} in Young Sound during a 2 months longer season of open water [*Sejr et al*., 2011]. The mismatch between our two CO_2 exchange approaches could partly be explained by the horizontal advection of surface water or supply of CO_2 from land-derived freshwater, which we have not taken into account.

5. Conclusions

The influence of freshwater and sea ice on variability of the CO_2 system, ocean acidification (OA state), and air-sea CO_2 uptake in a marine-terminating glacial fjord was investigated. Our 2 year study during these contrasting years clearly showed that the freshwater supply and processes in relation to sea-ice formation (e.g., haline convection) preconditions and significantly affected the chemical characteristics in the fjord. We also found that buffering components as carbonate ions in the drainage basin had the potential to affect the magnitude of change caused by increased ocean CO_2. The study indicates that increased supply of freshwater (land-derived and glacial drainage water) changes the ocean from a CO_2 source to a CO_2 sink. Our study supports previous findings that increased freshwater provides a positive feedback to ocean acidification (decreases Ω). However, fjords with freshwater originating from glacial drainage on carbonate and silicate-rich bedrock provide a partly negative feedback (or less positive feedback) on further ocean acidification. Moreover, the increased buffer capacity results in an increased potential for atmospheric CO_2 uptake, which will provide a positive feedback to OA on a longer time scale. The mass and volume of the Svalbard glaciers are mainly affected by warming and increased precipitation, which in turn will result in more glacial water supply and freshening in the Arctic. Consequently, we can expect increased ocean acidification and decreased calcium-carbonate saturation state (dissolution state, Ω), which may possibly lead to

changes of the living conditions for calcifying marine organisms. However, there are few and short time series in the Arctic Ocean and little information on the seasonal variability of the OA state. By studying fjords with different dynamics such as contrasting years (sea-ice and freshwater conditions) and drainage-water chemistry, we can understand more of the feedback processes in a changing Arctic.

Acknowledgments

This is a project within the Fram Centre flagship research program "Ocean acidification and ecosystem effects in Northern waters" at the FRAM—High North Research Centre for Climate and the Environment, and we thank the Ministry of Climate and Environment, and the Ministry of Trade, Industry and Fisheries, Norway, for financial support. We acknowledge the Japan Society for Promotion of Science support for D.N. and Svalbard Science Foundation Field Grant support to M.C. (grant 1795), D.N. (grant 1881), and T.M. (EU Regional Development Foundation, project 3.2.0801.12-0044). G.N. is supported by the DFG by grant NE 1564/1-1 (SPP1158). Data will be publicly available on the Svalbard Integrated Earth Observing System (SIOS) www.sios-svalbard.org and metadata will also be available at RiS portal at www.researchinsvalbard.no within 5 years after publication, until then contact the corresponding author. We thank Norwegian Polar Institute logistics in Longyearbyen for support and safety training. We are particularly grateful to Jørn Dybdahl, Jago Wallenchus, Helene Hodal Lødemel, and Mikael Hedström for field assistance, Monica Votvik for boat assistance, and Britt Vaaja for laboratory assistance. We also thank the two anonymous reviewers for constructive comments improving the paper.

References

Apollonio, S. (1973), Glaciers and nutrients in Arctic seas, *Science*, *180*, 491–493.

Azetsu-Scott, K., and J. P. M. Syvitski (1999), Influence of melting icebergs on distribution, characteristics and transport of marine particles in an East Greenland fjord, *J. Geophys. Res.*, *104*(C3), 5321–5328.

Azetsu-Scott, K., A. Clarke, K. Falkner, J. Hamilton, E. P. Jones, C. Lee, B. Petrie, S. Prinsenberg, M. Starr, and P. Yeats (2010), Calcium carbonate saturation states in the waters of the Canadian Arctic Archipelago and the Labrador Sea, *J. Geophys. Res.*, *115*, C11021, doi:10.1029/2009JC005917.

Azetsu-Scott, K., M. Starr, Z.-P. Mei, and M. Granskog (2014), Low calcium carbonate saturation state in an Arctic inland sea having large and varying fluvial inputs: The Hudson Bay system, *J. Geophys. Res. Oceans*, *119*, 6210–6220, doi:10.1002/2014JC009948.

Benn, D. I., N. R. J. Hulton, and R. H. Mottram (2007), 'Calving laws', 'sliding laws' and the stability of tidewater glaciers, *Ann. Glaciol.*, *46*, 123–130.

Chierici, M., and A. Fransson (2009), $CaCO_3$ saturation in the surface water of the Arctic Ocean: Undersaturation in freshwater influenced shelves, *Biogeosciences*, *6*, 2421–2432.

Cottier, F. R., V. Tverberg, M. E. Inall, H. Svendsen, F. Nilsen, and C. Griffiths (2005), Water mass modification in an Arctic fjord through cross-shelf exchange: The seasonal hydrography of Kongsfjorden, Svalbard, *J. Geophys. Res.*, *110*, C12005, doi:10.1029/2004JC002757.

Cottier, F. R., F. Nilsen, M. E. Inall, S. Gerland, V. Tverberg, and H. Svendsen (2007), Wintertime warming of an Arctic shelf in response to large-scale atmospheric circulation, *Geophys. Res. Lett.*, *34*, L10607, doi:10.1029/2007GL029948.

Cottier, F. R., F. Nilsen, R. Skogseth, V. Tverberg, J. Skarðhamar, and H. Svendsen (2010), Arctic fjords: A review of the oceanographic environment and dominant physical processes, in *Fjord Systems and Archives*, edited by J. A. Howe et al., *Geol. Soc. Spec. Publ.*, 344, pp. 35–50, London, U. K., doi:10.1144/SP344.4.

Dallmann, W. K., Y. Ohta, S. Elvevold, and D. Blomeier (2002), Bedrock map of Svalbard and Jan Mayen, *Norsk Polarinstitutt Temakart 33*, Norwegian Polar Institute, Norway.

Dickson, A. G. (1990), Standard potential of the (AgCl(s) + 1/2H_2 (g) =Ag(s) + HCl(aq)) cell and the dissociation constant of bisulfate ion in synthetic sea water from 273.15 to 318.15 K, *J. Chem. Thermodyn.*, *22*, 113–127.

Dickson, A. G., C. L. Sabine, and J. R. Christian (2007), Guide to best practices for ocean CO_2 measurements, chap. 4, pp. 23–78, *PICES Spec. Publ.*, *3*.

Evans, W., J. T. Mathis, and J. N. Cross (2014), Calcium carbonate corrosivity in an Alaskan inland sea, *Biogeosciences*, *11*, 365–379, doi:10.5194/bg-11-365-2014.

Forwick, M., T. O. Vorren, M. Hald, S. Korsun, Y. Roh, C. Vogt, and K.-C. Yoo (2010), Spatial and temporal influence of glaciers and rivers on the sedimentary environment in Sassenfjorden and Tempelfjorden, Spitsbergen, *Geol. Soc. Spec. Publ.*, *344*, 163–193, doi:10.1144/SP344.13.

Fransson, A., M. Chierici, L. G. Anderson, I. Bussman, E. P. Jones, and J. H. Swift (2001), The importance of shelf processes for the modification of chemical constituents in the waters of the eastern Arctic Ocean: Implication for carbon fluxes, *Cont. Shelf Res.*, *21*, 225–242.

Fransson, A., M. Chierici, L. A. Miller, G. Carnat, H. Thomas, E. H. Shadwick, S. Pineault, and T. M. Papakyriakou (2013), Impact of sea ice processes on the carbonate system and ocean acidification state at the ice-water interface of the Amundsen Gulf, Arctic Ocean, *J. Geophys. Res. Oceans*, *118*, 7001–7023, doi:10.1002/2013JC009164.

Gattuso, J.-P., and L. Hansson (2011), *Ocean Acidification*, Oxford Univ. Press, N. Y.

Gerland, S., and A. Renner (2007), Sea ice mass balance monitoring in an Arctic fjord, *Ann. Glaciol.*, *46*, 435–442.

Gillet, P., C. Biellmann, B. Reynard, and P. McMillan (1993), Raman spectroscopic studies of carbonates part I: High-pressure and high-temperature behaviour of calcite, magnesite, dolomite and aragonite, *Phys. Chem. Miner.*, *20*(1), 1–18.

Grasshoff, K., K. Kremling, and M. Ehrhardt (2009), *Methods of Seawater Analysis*, 3rd ed., John Wiley, N. Y.

Hagen, J. O., O. Liestøl, E. Roland, and T. Jørgensen (1993), Glacier atlas of Svalbard and Jan Mayen, *Norsk Polarinstitutt Meddelelser 129*, 141 pp.

Hanna, E., J. Cappelen, X. Fettweis, P. Huybrechts, A. Luckman, and M. H. Ribergaard (2009), Hydrologic response of the Greenland ice sheet: The role of oceanographic warming, *Hydrol. Processes*, *23*, 7–30.

Hjalmarsson, S., K. Wesslander, L. G. Anderson, A. Omstedt, M. Pertillä, and L. Mintrop (2008), Distribution, long-term development and mass balance calculation of total alkalinity in the Baltic Sea, *Cont. Shelf Res.*, *28*, 593–601.

Holland, D. M., R. H. Thomas, B. De Young, M. H. Ribergaard, and B. Lyberth (2008), Acceleration of Jakboshavn Isbræ triggered by warm subsurface ocean waters, *Nat. Geosci.*, *1*, 659–664.

Kohler, J., T. D. James, T. Murray, C. Nuth, O. Brandt, N. E. Barrand, H. F. Aas, and A. Luckman (2007), Acceleration in thinning rate on western Svalbard glaciers, *Geophys. Res. Lett.*, *34*, L18502, doi:10.1029/2007GL030681.

Lydersen, C., et al. (2014), The importance of tidewater glaciers for marine mammals and seabirds in Svalbard, Norway, *J. Mar. Syst.*, *129*, 452–471.

MacLachlan, S. E., F. R. Cottier, W. E. N. Austin, and J. A. Howe (2007), The salinity $\delta^{18}O$ water relationship in Kongsfjorden, western Spitsbergen, *Polar Res.*, *26*, 160–167, doi:10.1111/j.1751-836.9.2007.00016.x.

Mattsdotter-Björk, M., A. Fransson, A. Torstensson, and M. Chierici (2014), Ocean acidification state in western Antarctic surface waters: Controls and interannual variability, *Biogeosciences*, *11*, 57–73, doi:10.5194/bg-11-57-2014.

Millero, F. J. (2013), The carbonate system, in *Chemical Oceanography*, edited by F. J. Millero, 4th edition, chap. 7, 571 pp., CRC Press, Boca Raton, Fla.

Moholdt, G., J. O. Hagen, T. Eiken, and T. V. Schuler (2010), Geometric changes and mass balance of the Austfonna ice cap, Svalbard, *Cryosphere*, *4*, 21–34.

Morison, J., R. Kwok, C. Peralta-Ferriz, M. Alkire, I. Rigor, R. Andersen, and M. Steele (2012), Changing Arctic Ocean freshwater pathways, *Nature*, *481*, 66–70, doi:10.1038/nature10705.

Mucci, A. (1983), The solubility of calcite and aragonite in seawater at various salinities, temperatures and at one atmosphere pressure, *Am. J. Sci.*, *283*, 781–799.

Nehrke, G., and J. Nouet (2011), Confocal Raman microscope mapping as a tool to describe different mineral and organic phases at high spatial resolution within marine biogenic carbonates: Case study on Nerita undata (Gastropoda, Neritopsina), *Biogeosciences*, *8*(12), 3761–3769, doi:10.5194/bg-8–3761-2011.

Nilsen, F., F. Cottier, R. Skogseth, and S. Mattsson (2008), Fjord–shelf exchanges controlled by ice and brine production: The interannual variation of Atlantic Water in Isfjorden, Svalbard, *Cont. Shelf Res.*, *28*, 1838–1853.

Nuth, C., G. Moholdt, J. Kohler, and J. O. Hagen (2010), Svalbard glacier elevation changes and contribution to sea level rise, *J. Geophys. Res.*, *115*, F01008, doi:10.1029/2008JF001223.

Pierrot, D., E. Lewis, and D. W. R. Wallace (2006), MS Excel program developed for CO_2 system calculations, *ORNL/CDIAC-105*, Carbon Dioxide Inf. Anal. Cent., Oak Ridge Natl. Lab., U.S. Dep. of Energy, Oak Ridge, Tenn.

Raven, J., et al. (2005), *Ocean Acidification Due to Increasing Atmospheric Carbon Dioxide*, policy document 12/05, Royal Soc., London, U. K.

Redfield, A., B. H. Ketchum, and F. A. Richards (1963), The influence of organisms on the composition of sea water, in *The Sea*, vol. 2, edited by M. N. Hill, pp. 26–77, Interscience, N. Y.

Rignot, E., M. Koppes, and I. Velicogna (2010), Rapid submarine melting of the calving faces of West Greenland glaciers, *Nat. Geosci.*, *3*, 187–191.

Robbins, L., J. G. Wynn, J. T. Lisle, K. Y. Yates, P. O. Knorr, R. H. Byrne, X. Liu, M. C. Patsavas, K. Azetsu-Scott, and T. Takahashi (2013), Baseline monitoring of the Western Arctic Ocean estimates 20% of Canadian Basin surface waters are undersaturated with respect to aragonite, *PLoS One*, *8*(9), doi:10.1371/journal.pone.0073796.

Roy, R. N., L. N. Roy, K. M. Vogel, C. Porter-Moore, T. Pearson, C. E. Good, F. J. Millero, and D. M. Campbell (1993), The dissociation constants of carbonic acid in seawater at salinities 5–45 and temperatures 0–45°C, *Mar. Chem.*, *44*, 249–267.

Roy, R. N., L. N. Roy, K. M. Vogel, C. Porter-Moore, T. Pearson, C. E. Good, F. J. Millero, and D. M. Campbell (1994), Erratum for: The dissociation constants of carbonic acid in seawater at salinities 5–45 and temperatures 0–45°C, *Mar. Chem.*, *45*, 337.

Rysgaard, S., R. N. Glud, M. K. Sejr, J. Bendtsen, and P. B. Christensen (2007), Inorganic carbon transport during sea ice growth and decay: A carbon pump in polar seas, *J. Geophys. Res.*, *112*, C03016, doi:10.1029/2006JC003572.

Sejr, M. K., D. Krause-Jensen, S. Rysgaard, L. L. Sørensen, P. B. Christensen, and R. N. Glud (2011), Air-sea flux of CO_2 in arctic coastal waters influenced by glacial melt water and sea ice, *Tellus, Ser. B*, *63*, 815–822.

Skogseth, R., P. M. Haugan, and M. Jakobsson (2005), Dense-water production and overflow from an arctic coastal polynya in Storfjorden, in *The Nordic Seas: An Integrated Perspective—Oceanography, Climatology, Biogeochemistry, and Modeling*, edited by H. Drange et al., pp. 73–88, AGU, Washington, D. C.

Svendsen, H., et al. (2002), The physical environment of Kongsfjorden-Krossfjorden, an Arctic fjord system in Svalbard, *Polar Res.*, *21*, 133–166.

Wanninkhof, R. H. (1992), The relationship between gas exchange and wind speed over the ocean, *J. Geophys. Res.*, *97*, 7373–7381, doi:10.1029/92JC00188.

Yamamoto-Kawai, M., F. A. McLaughlin, E. C. S. Carmack, S. Nishino, and K. Shimada (2009), Aragonite undersaturation in the Arctic Ocean: Effects of ocean acidification and sea ice melt, *Science*, *326*, 1098–1100, doi:10.1126/science.1174190.